POLYPUBLIE
Polytechnique Montréal

POLYTECHNIQUE MONTRÉAL
UNIVERSITÉ D'INGÉNIERIE

Document en libre accès dans PolyPublie
Open Access document in PolyPublie

Document publié chez l'éditeur officiel
Document issued by the official publisher

A Model Approach for Binder Selection in Binder Jetting

Sergio I. Yanez Sanchez* [1], Martin D. Lennox[1], Daniel Therriault[2], Basil D. Favis[1], Jason R.

Tavares*[1]

[1] CREPEC, Department of Chemical Engineering, Polytechnique Montreal, Montréal, QC,

H4T 1J4, Canada

[2] CREPEC, Department of Mechanical Engineering, Polytechnique Montreal, Montréal, QC,

H4T 1J4, Canada

Abstract

Three binders, polyvinyl alcohol (PVA), polyvinylpyrrolidone (PVP) and polyacrylic acid
(PAA) are studied to elucidate the principal fundamental features giving rise to an excellent
binder in a polymer-stainless steel particle array, used in the context of binder jetting. Using
an out-of-printer screening approach, samples were compared based on compression tests,
specifically the 0.2 % yield strength as a function of void volume fill factor, ϕ, leading to a
quasi-sigmoidal generalized curve for green body strength development. PVA demonstrated a
strong tendency to form inter-particle bridges at low ϕ and the highest rise in strength, while
PAA samples exhibited a lower tendency to form inter-particle bridges and a weak exponential
rise in strength. This paper relates these behaviors to polymer strength, capillary properties and

polymer-metal interactions and ultimately provides a rigorous selection process for binder efficacy.

Introduction

Binder jetting (BJP) is an advanced manufacturing technique where the alternating deposition of a metal powder bed, then printing of a polymeric binder are repeated until a three-dimensional part is formed. The resulting piece is called green body. It is composed of powder particles held together by the binder. To obtain a pure metallic part, the piece must be treated thermally in two steps: first, to remove all the binder by pyrolysis and then, to sinter the powder particles. It is one of the most promising techniques, industrially, as it possesses many advantages over the other additive manufacturing techniques: it has a broader material versatility (including polymers, ceramics, food and metals), one of the highest resolutions and speeds, one of the lowest building volume restrictions and consumes less energy [1-4].

Despite all of its advantages, BJP is only the fourth most used additive manufacturing technique for metallic printing [5]. Even though, in some applications, BJP can compete with the most popular techniques [1], the main disadvantage holding it back is related to the mechanical properties of the pieces. During their fabrication, green bodies can be fragile [6, 7], which can cause high production losses. Additionally, if the binder leaves high amounts of residue after debinding, the final pieces can have poor properties due to high porosity and impurity content [1, 2, 8]. Therefore, the binder choice is of capital importance in the BJP process. However, binder

selection is mostly done by trial and error, a consequence of a lack of understanding of the fundamental interactions that make a good binder.

Theoretical framework

When the binder is printed, it penetrates into the powder bed and fills all the interparticle voids. The binder is all interconnected at that point. As the solvent dries, capillary forces drive the binder towards the necking regions: interparticle contact points [9, 10]. Ideally, the process finishes by the deposition of all the binder in the inter-particle contact points, such that the full strength of the binder is used to maintain part integrity [10]. However, if the binder is too concentrated, the ingredients might start depositing onto the particles before the liquid is fully localized at the necking regions (early precipitation) [11]. Additionally, depending on how it wets the powder surface, the binder might deposit in three different ways [12]: (1) the nonwetting state, where the polymer is randomly located on the surface of the particles; (2) the pendular state, where the polymer locates at the necking region between particles; and (3) the coated state, where the polymer is evenly distributed on the surface of the particle. Pendular and coated states can be obtained if the contact angle of the binder on the powder is lower than 90 °. In other words, one can obtain a pendular and coated behavior if the binder wets the metal surface adequately. However, if the binder's viscosity is high, the coating behavior is also obtained, as a high viscosity liquid can resist the capillary pressures that pull the binder towards the necking regions.

The physicochemical properties of the binders can be characterized thanks to the dimensionless capillary number Ca [13]:

$$Ca = \frac{\mu\eta}{\gamma}$$ (1)

were η, μ and γ are the viscosity, the velocity of the fluid in the powder bed and the surface tension, respectively. The capillary number Ca is considered as an indicator of the capacity of the binder to undergo a capillary displacement. This dimensionless number highlights the relation between the surface tension and the viscosity in a capillary flow [13]. If Ca increases the capillary flow is less favored.

The resulting green bodies are granular materials held together by interparticle bonds. The bonds in one part of the piece can break without transmitting the stress to the other bonds. This means that interparticle connections are what gives strength to the pieces, regardless of the individual strength of the particles [14, 15], strength being the capacity of the body to withstand a load. Based on geometric considerations, Onoda estimated the volume of binder between two spherical particles to be [12]:

$$V_{bridge} = \frac{\pi r^2 h}{2}$$ (2)

where r is the radius of the bond and h, its length (Figure 1 a). This model also proposes a method to calculate the number of bonds in a green body, assuming that the particles are spherical and mono-sized:

$$n = \frac{V_{metal}}{V_{particle}} \frac{k}{2} = \frac{V_{metal}}{\frac{4}{3}\pi R^3} \frac{\pi}{2p} \tag{3}$$

where V_{metal} is the total volume of metal in the green body p, the volume fraction of pores and $k = \pi/p$ the average number of neighbour particles around one particle. Finally, with these and other geometric considerations and assuming that the bonds are all pendular and that the binder is all located at the necking regions, Onoda proposed that the green strength was proportional to the square root of the volume of binder in the piece and to the binder strength.

The strength of a single particle-particle bridge can be also modelled as the strength of a hollowed cylindrical beam:

$$F_{bond} = \frac{\sigma_{binder}\pi(r^4 - r_0^4)}{4hr}. \tag{4}$$

where F is the maximum load, r, the outer radius of the bond, r_0, the inner radius and h, the length of the bridge, as depicted in Figure 1 a. Figure 1 b shows the trend of equation (4).
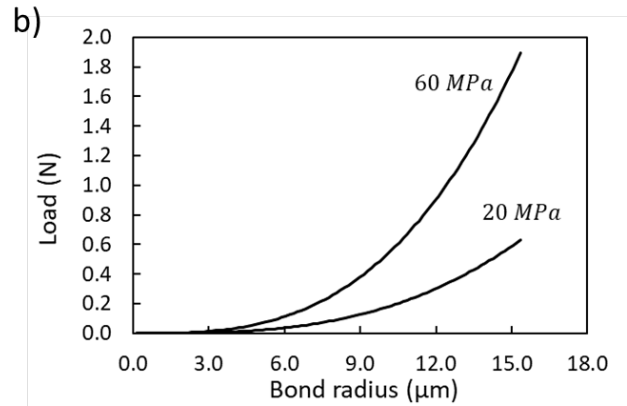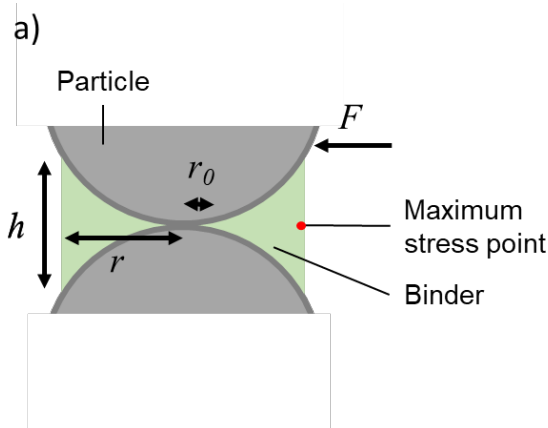
Figure 1. Cylindrical beam model: a) Schematics of the beam model applied to a pendular bridge. b) Bond strength as a function of bond radius for a single bond according to equation (4) for two different binder strengths.

Among the eight types of binding materials [10, 16], organic polymer-based binders are often preferred as they are easily decomposed during debinding. Also, they do not require a specific reaction to work and can bind a large variety of materials. However, although the strength of the green bodies rises as the binder content in the pieces increases, the quality of the final metallic piece decreases, as residual carbon may cause deviations from standardized metal compositions. In other words, a binder that strongly holds the piece with the lowest possible amount of binder is desired. Research on binding materials is mainly focused in improving green strength, but does not systematically consider effects of concentration, and the different regimes this may bring about. Indeed, strength improvement is pursued by using new polymeric materials such as phenolic resin [17], by tailoring the polymer chain's architecture [18], and by tailoring the polymer chain's chemistry [19].

To the best of our knowledge, there exists only one binder selection algorithm to develop binders for BJP [16]. A few selection algorithms from other branches of inkjet printing such as circuitry printing [20] could potentially be adapted to some level for binder selection. However, these existing algorithms mostly focus on meeting the printing process requirements and not on the interactions between the binder and the particles, necessary to predict green body performance.

Therefore, the main objective of this research is to develop guidelines for binder selection based on polymer – polymer and polymer – metal interactions, while considering the effect of binder concentration.

Materials and Methods

Powder, Polymers and additives

Stainless steel 316L powder with average diameter of 13 μm was purchased from CNPC Powder and used without any treatment. The density of the pure metal is 7.9 g/cm^3 and the surface mean diameter D_{21} = 15 μm. See supplementary information S1 for additional details on the powder material (Figure S1. BSE SEM images of the SS 316L powder and Table S1. Composition of the SS 316L powder).

Three different polymers were used in this study: polyvinylpyrrolidone (PVP), polyvinyl alcohol (PVA) and polyacrylic acid (PAA). These polymers were selected as they have been used previously as binders in binder jetting and other manufacturing techniques, and are thus useful to gain access to comparative data [4, 18, 21-30]. Additionally, these polymers contain different polar functional groups and have different mechanical properties that confer contrasting properties to the final green bodies. Finally, they can be used to produce ecofriendly binders as they are soluble in water. Indeed, water is retained as the dispersing medium used in this study because of its non-toxic nature, and because it wets SS 316L (contact angle between water and stainless steel is around 54 ° [31]). PVP 40k, PVA 9-10k (80 % hydrolyzed) and PAA 100k 35 wt. % water solution, were purchased from Sigma-Aldrich and were used without further

purification. Here, "40 k", "9-10k" and "100k" are the molecular weights in g/mol for the three polymers. In the case of PVA, the hydrolysis percentage indicates the amount of hydroxyl functional groups in the chain. The densities of the polymers are 1.25 g/cm³, 1.27 g/cm³ and 1.41 g/cm³ for the PVP, PVA and PAA, respectively.

Binder preparation and characterization

Binders with polymer concentrations ranging from 3 wt. % to 50 wt. % were prepared. The polymers were added to DI water and stirred with a magnetic stir bar for 1 - 24 h in a hot-water bath at 60 ° C (to accelerate dissolution). Finally, the binders were filtered with 0.45 μm Millipore MIL-SLHV033RB filters, except for the 50 wt. % binder, as it was too viscous for the filters.

The density of the binders was measured by micro-pipetting 0.33 ml of binder (+/- 0.003 ml) and weighting it on a microbalance ((+/- 0.0001 g) – values reported are the average of 5 tests, along with the 95 % confidence interval (95% C. I). The dynamic viscosity of the binders was measured with an Anton-Paar MCR501 rheometer, using a DG26.7 test geometry and a C-PTD200-SN81036684 Pelletier module (23 ℃). The measurements were done in rotation with decreasing shear rates (1000 – 0.01 s-1). Surface tension was measured with a Data Physics tensiometer OCA 15 EC using the pendant drop technique.

Sample preparation

Samples were prepared with an out-of-printer approach in order to bypass the optimisation of printing parameters for every binder and to avoid the printhead limitations concerning

viscosity and surface tension. This avenue allows us to separate the printer parameters' impact on the green bodies' properties from the fundamental interactions. It also allows us to study the full range of final dried binder concentrations in the green body, from 0 to 100 wt %. Most of the works exploring binder concentration in binder jetting are limited to small concentration variations due to the constraints of the printhead and the binder's printability [17, 18, 32]. Thus, this approach is not an analogy to the printing process. It is a model work that facilitates the analysis of the interactions of the binder and the metal particles and helps screen various binders, while keeping the printer free for production during binder development.

The sample preparation follows the steps in Figure 2. First, the binder and the metallic powder are mixed on a crucible until the formation of a malleable paste (Figure 2 a). The paste is then put a cylindrical mould (1 cm of height, 1 cm of diameter). The mould consists of two 3D printed PLA pieces (side walls) and a microscope slide (bottom support). These pieces are held together with an elastic band (Figure 2 b). Once the paste is molded, it is dried in an oven at 60 °C for a day and subsequently demoulded (Figure 2 c).
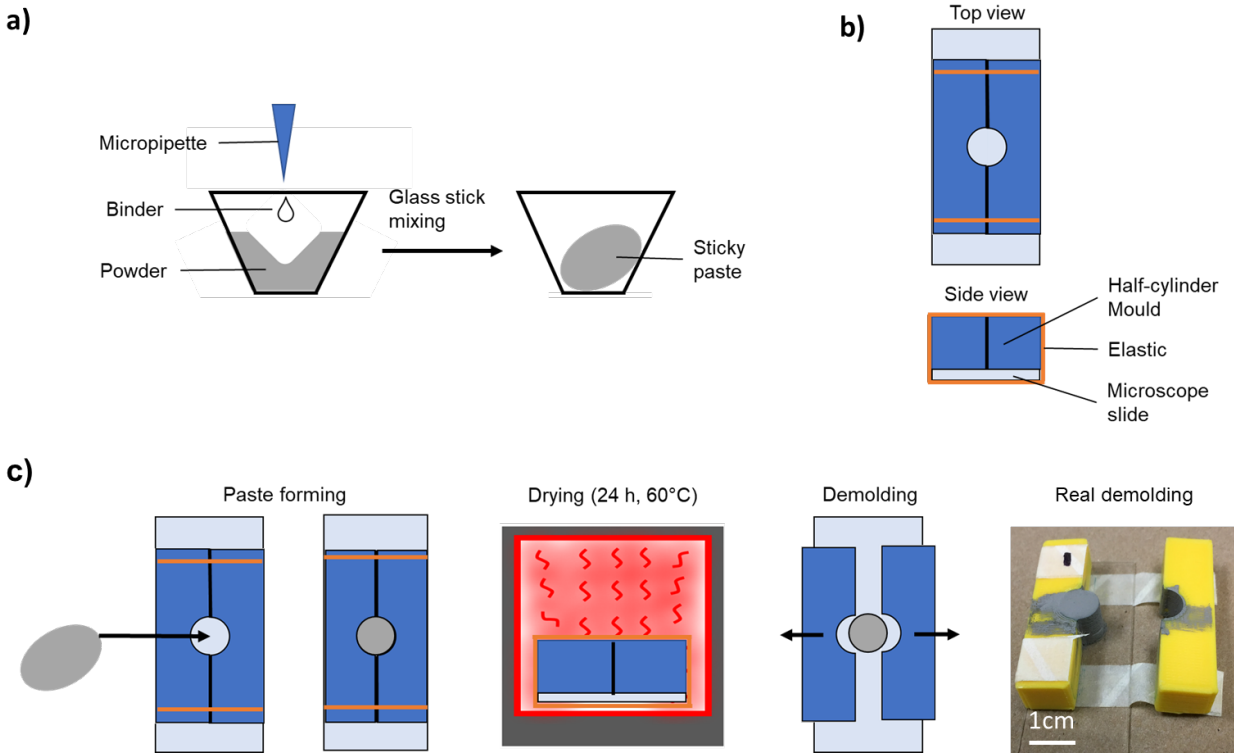
Figure 2 Green body preparation schematic: a) paste preparation, b) mould assembly and c) sample preparation.

To characterize the amount of binder in the green bodies, a parameter called fill factor ϕ was defined as the ratio between the volume of dried binder, V_{binder}, and the volume of the piece that is not occupied by the metal powder, V':

$$\Phi = \frac{V_{binder}}{V_{piece} - V_{metal}} = \frac{V_{binder}}{V_{air} + V_{binder}} = \frac{V_{binder}}{V'} \tag{5}$$

were V_{piece} is the volume of the green body (metal + binder + air), V_{metal}, the volume of metal as if the powder was one full metallic piece and V_{air}, the volume of air. The binder concentration C_b is the polymer concentration in the liquid solution:

$$C_b = \frac{m_{polymer}}{m_{solvent} + m_{polymer} + m_{additives}} \qquad (6)$$

while the green concentration Cg is the amount of solid polymer in the piece, after the evaporation of all the liquid:

$$C_g = \frac{m_{polymer}}{m_{piece}} \qquad (7)$$

where m stands for "mass".

The volume of metal in the green bodies was practically constant through the different ϕ values. In average, it is 0.43 ± 0.02 cm³ (error is a 95 % C. I.). However, depending on the C_b values and the corresponding viscosities of the binders, the first step (Figure 2a) is modified. Low C_g samples were made with C_b values between 3 and 35 wt. %. In such case, the green bodies were made by adding 0.33 ml of binder solution to 5 g of powder. Binder volumes were measured with a micropipette and the powder weight was measured with a microbalance. This resulted in C_g values between 0.2 and 2 wt. %. Note that C_b values below 3 wt. % were not used, as they resulted in green bodies that broke during the demoulding step. More details on the resulting binder distribution in the green bodies are available in the supporting information S2 (Figure S2. Binder distribution on a green body with respect to the height of the piece.).

For the medium C_g samples, a $C_b = 50$ wt. % was used. The proper amount of binder solution was added to the powder by weight, using a microbalance, as the binder's viscosity was too high to use a pipette. This resulted in a C_g value of 5 wt. %.

Green bodies with high C_g (50 wt. %) were prepared by hand-mixing the binder ingredients and the powder in a crucible. In other words, the binder was not prepared as a solution. The

ingredients were all manually mixed with the powder at the same time. Once moulded, dried and demoulded, these samples were heated in a convection oven (Precision Freas 625S Oven from Thermo Scientific) to sinter the polymer granules that were not dissolved during the hand mixing stage. These sampled were first held at 60 °C for 1 h. Then, the temperature was increased in steps of 10 °C every 10 minutes up to 180 °C (90 % the melting temperature of PVA). The oven was then turned off to let the samples cool down (30 min).

Finally, pure polymer samples were obtained with a similar technique as that of the 50 wt. % green concentration samples. To form the paste, the polymer granules were hand-mixed with water in a crucible without any metallic powder. Once demoulded the samples were heat treated to sinter the polymer: 60 °C for 1 h, followed by steps of 10 °C every 10 minutes up to 190 °C before and a cool down of 30 min.

The maximum temperature of the heat treatment of the 50 wt. % green concentration samples was lower than that of the pure polymer samples because the metallic particles improved the heat distribution in the piece. If these samples were held at higher temperatures, the polymer would completely melt.

To recapitulate, we analyzed four types of bodies. They were classified with respect to the paste formation technique we used to prepare them: low concentration, medium concentration, high concentration, and pure polymer. Table 1 summarizes the paste formation techniques and indicates the binder concentrations (C_b) used and the final green concentrations (C_g) obtained.

Mass and dimensions

The mass and dimensions of the green bodies were measured with a caliper (+/- 0.01 mm) and a microbalance (+/- 0.0001 g). Measurements were repeated 3 times for every sample. These results were used to calculate the density of the green bodies and to define its 95% C.I. The densities of pure SS 316L (7.9 g/cm³) and pure PVA (1.27 g/cm³, 9-10 kg/mol, 80 % hydrolyzed) were used as references to calculate the relative density.

Table 1. Summary of C_b, C_g and paste compositions.

Type of sample	Paste composition	C_b	C_g
Low concentration	0.33 ml of binder + 5 g of powder	3 – 35 wt. %	0.2 – 2 wt. %
Medium concentration	0.56 g of binder + 5 g of powder	50 wt. %	5.35 wt. %
High concentration	2.5 g polymer granules + 2.5 g metal + water*	-	50 wt. %
Pure polymer	3 g polymer granules + water*	-	100 wt. % (without metal particles)

* Enough water to form a malleable paste.

Mechanical testing

The samples were tested in compression (Figure 3 a) with an MTS Insight electromechanical testing system with a strain rate of 1 mm/min and a load cell of 1kN, 20 kN or 50kN, depending on the green strength. The tests were done on 3 replicates or more (N ≥ 3).

From the compression test data, the 0.2 % yield strength was calculated (Figure 3 b) and a 95% C.I. was defined. The 0.2 % yield strength was preferred to characterise the green strength over the yield point because the green bodies did not show a clear transition between elastic and plastic behavior [33-35]. The 0.2 % offset value was also preferred over the ultimate strength since a piece that bears a load higher than the 0.2 % yield strength is already deformed and thus unusable. Therefore, the maximum load that a green body can handle should be estimated using this value and not the ultimate strength or the yield point. Figure 3 c and d show the difference between the samples before and after the compression test.
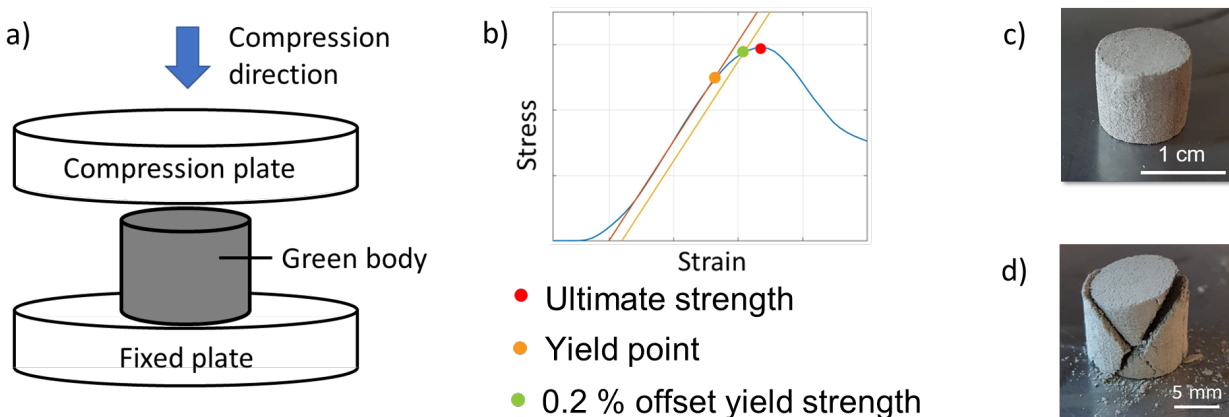

Figure 3. Green body strength analysis by compression test (N ≥ 3): a) mechanical test schematic, b) data analysis schematic, c) green body before compression and d) green body after compression.

Scanning electron microscopy

SEM images were taken in BSE mode to analyse the interactions of the binder with the powder and the failure mechanisms. The images were taken with a JEOL JSM 7600F microscope, at a potential of 5 kV, a working distance between 13 and 17 mm and an emission current of 219.2 μA. In the case of high concentration PVP samples ($C_g > 1$ wt. %), the charging effect forced the use of an electroplated gold film. In all the other cases, no surface treatment was required. The surfaces were not smoothened because the samples were too fragile. With the help of ImageJ, the length of the interparticle bridges was measured on SEM BSE images. Six bridges were measured, and every bridge was measured 6 times. See supplementary information S3 for more details on the interparticle bridge length measurement (Figure S3. Bond length measurement with ImageJ).

Results & Discussion

Binder concentration and mechanical properties

PVA

The 0.2 % yield strength of PVA green bodies is plotted against the fill factor in Figure 4. The trend resembles a quasi-sigmoidal curve, which can be divided in two main regions: an exponential-like increase of strength from 2.1 to 18.3 % and a tail-off, a long reach of the maximum strength from 18.3 to 93 %. Even though the strength increase is slower after the inflexion point at 18.3 %, it continues rising significantly up to around 50 % before reaching a plateau around 70 %. The maximum strength (60 ± 10 MPa) is that of pure polymer samples (i.e. containing no metal particles).
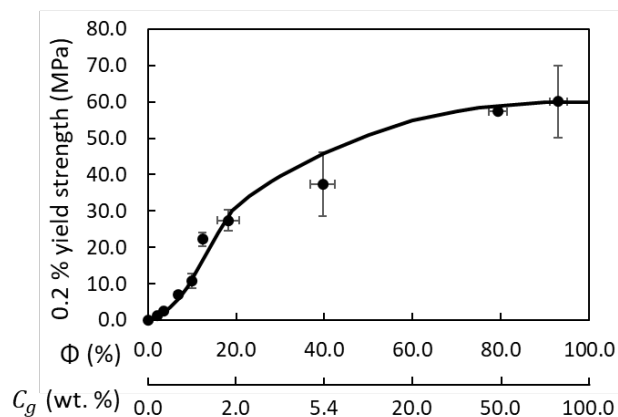
Figure 4. 0.2 % yield strength of PVA green bodies as a function of ϕ and C_g (solid line to guide the eye). Error bars are 95% C. I.

The inflexion point arrives at very low C_g values: a ϕ value of 18.3 % corresponds to a C_g value of 1.92 wt. % and $\phi = 39.6$ % corresponds to $C_g = 5.35$ wt. %. In other words, the strength increases until the point where the binder replaces a significant fraction of the air volume in the piece and that happens around $C_g = 20$ wt. %.

Based on the data on Figure 4, the model curve of the green strength as a function of Φ is proposed in Figure 5. The behavior of the green bodies as a function of binder content is divided into three regions, limited by the red points and dashed lines. Region A corresponds to the range of concentrations where binder starts accumulating in the interparticle regions without forming interparticle bridges. Therefore, no green bodies can be formed at this stage. The transition to Region B occurs when the first binder bridges are formed. At that point, the strength of the pieces starts rising in an exponential-like manner. Finally, Region C is a long reach for the maximum strength, the pure polymer strength.
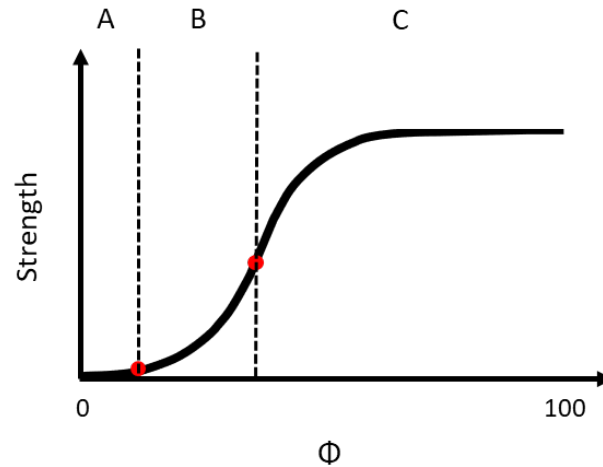
Figure 5 Strength as a function of the fill factor model curve. Region A: induction regime where no interparticle bridges have formed; region B: interparticle bridge network formation and bond coarsening; region C: tail off to pure polymer properties

Onoda's theoretical model of green strength predicts a fast increase at the beginning of the strength-concentration curve followed by a plateau [12]. However, it does not account for the exponential shape of the curve. That exponential trend at low binder concentrations has been observed experimentally before [17]. However, due to printhead limitations in BJP, only small variations of concentration were previously studied. For this reason, the trends seem linear in some studies [18, 36]. Considering the bridges as hollowed cylindrical beams is more in agreement with the experimental data obtained, in terms of the shape of the trend. Figure 1b clearly reveals the exponential-like increase of the strength of a single bond as its radius increases, the radius being directly linked to ϕ. Since the strength of a green body is the sum of the contributions of every interparticle bridge (eq. 8), it is reasonable to obtain an exponential-like increase for the green strength too.

$$\sigma_{green} = \frac{1}{A_{green}} \sum_i F_{bond,i} n_i \qquad (8)$$

This said, equation (8) overestimates the real green strength because it does not consider the effect of stress inhomogeneities and crack nucleation and propagation mechanics. Additionally, it does not consider the impact of the binder location in the piece. Nonetheless, one can conclude that the exponential-like increase is driven by the interparticle bridge coarsening.

The exponential-like increase takes place up to Φ = 18.3 % (in PVA), where the bonds start touching each other. By dividing the binder volume of the piece by the number of bridges (eq.(3)), one can obtain the volume of binder between particles, assuming that all the binder is located at the necking region. With that information for the samples at 18.3 %, the inflexion point, equation (2) tells us that the interparticle bridges' length is approximately 1.10 μm. The real length of the bonds, measured with the help of SEM images for 6.9 % samples, is 0.62 ± 0.05 μm (error is a 95 % C. I.). The bridge size measurements were done on 6.9 wt. % samples since the interparticle bonds at that concentration are more defined. A bridge length of 0.62 μm is reasonably close to 1.10 μm considering that all the binder is located in the interparticle regions only in ideal cases. In reality, there is always binder deposition in non-optimal locations. In Figure 7 c, one can see that the 12.4 % sample has already a significant amount of binder outside the necking regions even though, the interparticle zones are not saturated (white arrows). This is normal, as that sample is close to the inflexion point concentration.

Therefore, the inflexion point is the point where the interparticle necking regions get saturated and the binder starts depositing elsewhere.

With that in mind, the shape of the model curve in Figure 5 can be further explained. The exponential-like increase takes place due to the interparticle bridge coarsening and to an increasing number of interparticle bonds that are being formed. The formation of an interparticle solid network of metal particles linked by the binder is completed in Region B. Thus, binder jetted samples fall in this region. Additionally, the transition from region B to C takes place when the binder's fill factor in the metal powder is high enough to saturate the interparticle regions. At that point, interparticle bridges touch each other and the binder starts filling the remaining pores as the concentration increases. For that reason, Region C is a long tail-off that reaches the pure polymer strength.

Before the inflexion point ($\Phi = 18.3\ \%$), the relative density of the green bodies stays constant since the volume and mass of the polymer are negligible with respect to the volume of metal (Figure 6). After that point, the density of the bodies starts increasing, which also indicates that the necking regions are saturated and the pores between particles are being filled by the binder.
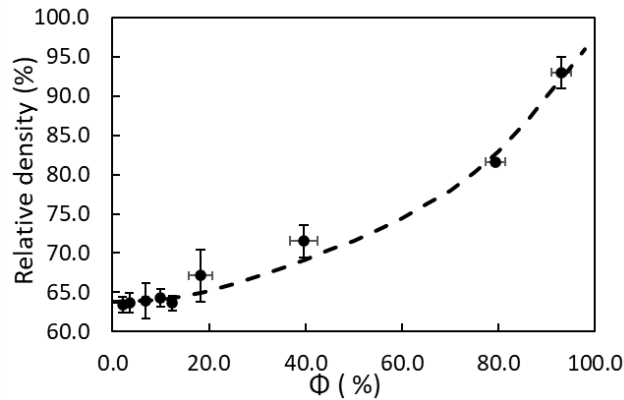
Figure 6. Relative density of PVA green bodies as a function of ϕ (dashed line to guide the eye). Errors are 95% C. I.

Comparing Figure 4 and Figure 6, one can see that for low ϕ values (0 to 18.3 %), the relative density stays constant even though the concentration and the strength increase. This is rarely seen in BJP, as changes in concentration are often achieved by changing the binder volume through the printing parameters. In other words, to change the final binder concentration of a piece, normally, the printing parameters such as saturation ratio or droplet volume are adjusted. This results in an increase of binder concentration in the final piece, but also in an increase of liquid binder volume. This increase of liquid in the green body results in a densification of the powder bed because of the action of capillary forces that pull the particles together [37]. For instance, Melcher et al. obtained a decrease of 4.4 % in the porosity of green bodies by increasing the printing liquid saturation from 0.21 g/cm^3 to 0.35 g/cm^3 [38]. However, the strength variation of the green bodies was not measured in that study. That said, other works have maintained the liquid saturation while changing the concentration of the binder, similar to the method used in this work [18, 32]. In the case of [18], an augmentation of C_b of 6 wt. % resulted in a

reduction of the green bodies' porosity of ˜ 5 % and an increase of green strength from 0.56 to 0.96 MPa. Therefore, binder concentration variations in the green body can result in a densification of the pieces for two reasons: increased capillary pressures and increased space filling in the bodies [32]. This is not the case in our method, as the different samples up to $\phi =$ 18.3 % maintained a similar density even if the binder concentration varied. Interestingly, those samples were prepared using the same liquid volume (0.33 ml), but different C_b values. Therefore, with our out-of-printer technique, the final dried binder content increased, but the powder packing density was unaffected. Hence, this method results in an increase of ϕ without having a significant impact on the relative density up to the inflexion point. Thus, this data shows that even if higher densities result in higher green strengths, the impact of binder concentration is much more important in BJP.

The relative density of the low ϕ bodies varies between 63 and 65 %, which is comparable to what can be obtained for SS 316L [17] and other types of SS [39] in the printing process, generally close to 60 %. It is important to notice that the density of the pure PVA samples was of 93 %, which indicates that these samples had a porosity of ˜7 %.

Figure 7 presents SEM micrographs of green bodies after compression tests for three different ϕ values. As the fill factor increases, the polymer is more and more visible (seen in these micrographs as dark areas, especially at particle contact points). Interestingly, the polymer is almost invisible in the lower concentration sample (Figure 7 a, ϕ=3.5%). However, its 0.2 % yield strength is 2.6 MPa, indicating that the polymer is located between the particles. As concentration increases, the shape of the binder bridges becomes more apparent. In Figure 7 b

(ϕ =6.9%), the circular and semi-circular binder marks are places where particles were bonded. Additionally, in the same figure, we can observe that the binder tends to interconnect the binder bridges. Slim binder lines identified with yellow arrows are connected to the annular marks, which indicates that there is a certain amount of binder that is not useful, i.e. that does not participate in interparticle bonding. The higher fill factor sample shows signs of polymer decohesion (Figure 7 c, ϕ = 12.4 %). Between the particles, the polymer seems to be torn (red arrows). It leaves two polymer sides with uneven, rough shapes. This implies that the PVA-SS 316L samples fail in the polymer phase, and not at the polymer-metal interface. Therefore, the interactions between the binder and the metal are stronger than those between the polymer chains. In other words, the strength of the green bodies is governed by the binder phase strength.
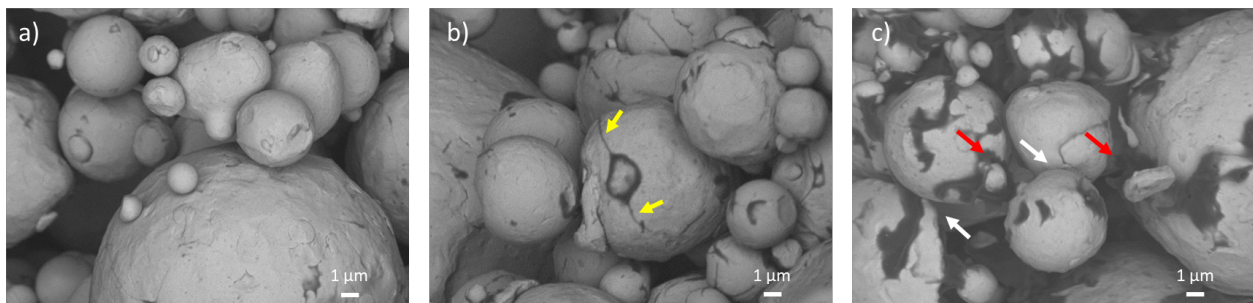

Figure 7. BSE SEM images of fractured PVA green bodies with different ϕ values: a) 3.5 %, b) 6.9 % and c) 12.4 % . Yellow arrows point at the slim binder lines coming out of the annular mark. Red arrows point at places where the polymer failed cohesively. White arrows point at interparticle necking regions.

The properties in solution of PVA could explain the presence of the binder lines observed in Figure 7 b. Normally, the binder forms a continuous matrix when it is liquid and as it dries, it is pulled towards the necking regions under the effect of capillary pressures and results in individual interparticle bridges (Figure 8 a). In this case, as the binder dries, it turns into a gel because the polymer concentration increases [40]. Through hydrogen bonding, PVA chains form a physically crosslinked network: the hydroxyl groups of one chain can react with the hydroxyl groups of other chains [41, 42]. For this reason, as the liquid dries, the cohesive energy of the hydrogel is sufficiently high to maintain the binder interconnected. Finally, when the binder is almost dry, the concentration of PVA reaches saturation, which makes it deposit even if it is not located at the necking regions [10] (Figure 8 b). This said, these interconnections are not maintained through all the piece and they become thicker in samples with higher binder concentration. At low concentrations they are not apparent.
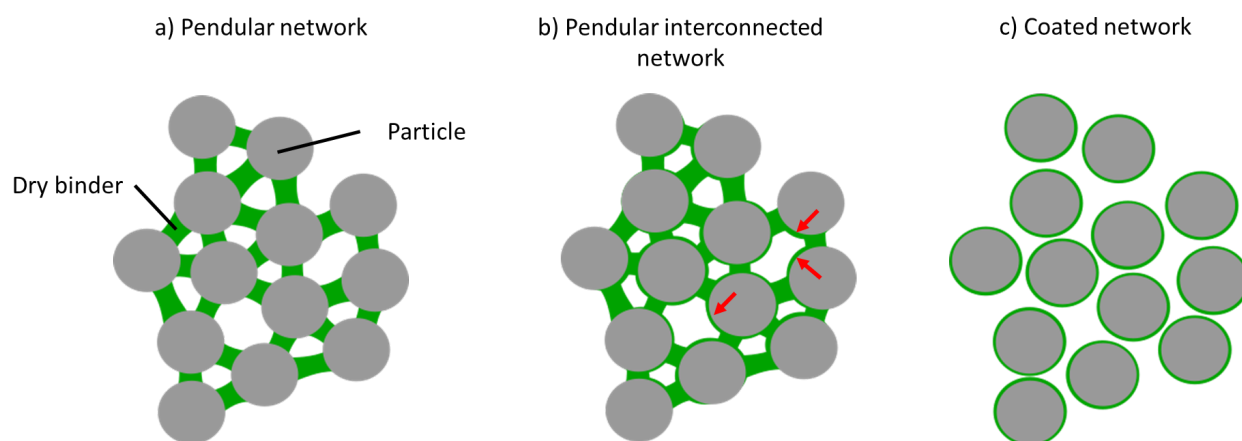

Figure 8. Binder-particle networks. a) Pendular network (preferred): all the interparticle bonds are pendular. b) Pendular interconnected network (less preferred): the pendular bridges are interconnected by thin binder lines (examples pointed with red arrows). c) Coated network

(not preferred): weak interparticle network due to the binder distribution. More binder is needed to form interparticle bridges.

PAA and PVP

In Figure 9, the 0.2 % yield strengths of PVP and PAA green bodies are compared to those of PVA samples for various fill factors. Interestingly, PVP and PAA also show an exponential-like increase, as proposed by the model curve. However, the strength increase is lower for PVP and even lower for PAA. According to the cylindrical beam model, it could be caused by the mechanical properties of the polymers. In fact, the mechanical strength of the binder has a direct impact on the increase rate of the strength (Figure 1 b). Tensile tests of pure PVA, PAA and PVP films indicate that the strengths of those polymers are 44 MPa (M_w = 26 kg/mol) [43], 27 MPa (M_w = 90 kg/mol) [44] and 16 MPa (M_w = 75 kg/mol) [45], respectively. As PAA and PVP have lower mechanical properties than PVA, it is normal that their strength increase is also lower. However, PVP gives better properties to the green bodies than PAA even if PAA is expected to be stronger based on pure properties.
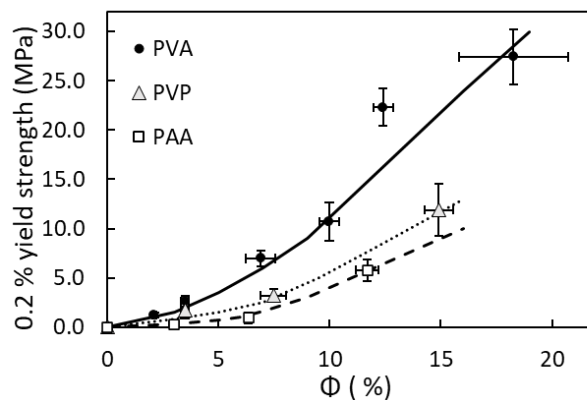
Figure 9. 0.2 % yield strength of green bodies made with PVA, PVP and PAA binders as a function of ϕ (solid and dashed lines to guide the eye). Errors are 95% C. I.

The binder distribution in the green bodies could explain why there is a switch of green properties with respect to pure polymer properties between PVP and PAA samples. The SEM images in Figure 10 show how these three binders behave and form inter-particle bridges in their respective green bodies. On one hand, PVP's behavior is similar to that of PVA. They both form pendular bridges and have annular marks where the particles were bonded. On the other hand, PAA tends to preferentially coat the metallic particles (Figure 8 c). At small concentrations (top images in Figure 10), the PAA sample contains annular marks where particles were bonded, but it also contains several non-annular marks all over the metallic surface. This means that a significant amount of binder is not participating in the inter-particle bridging, which reduces significantly the mechanical properties of the sample [12]. This behavior is therefore undesired. It explains why PVP gives more strength than PAA even if it has lower mechanical properties. The coating behavior of PAA is more apparent in the bottom images of

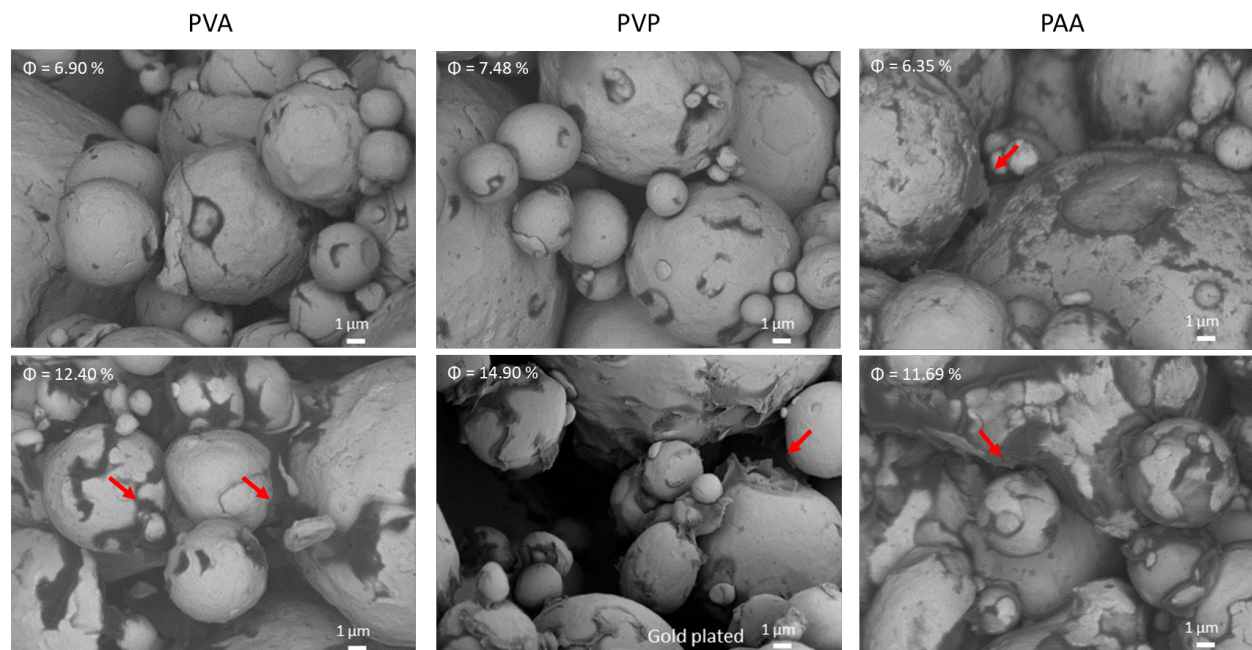Figure 10. One can clearly see that the particles in the PAA sample are completely coated by the binder.

Figure 10. BSE SEM images of PVA, PVP and PAA green bodies with different ϕ values. Red arrows point at places where the polymer failed cohesively.

As previously said, PVP and PVA display similar binder distributions. However, PVP does not tend to have interconnected bridges. It forms regular pendular bonds such as those depicted in Figure 8 a. this difference can be explained by the strength of attraction between the chains in solution. That interaction can be characterized with the help of the cohesive energy density (CED) [24]. In fact, PVP has a lower CED than PVA (305 J/cm³ for PVP, 519 J/cm³ for PVA [24] and 543 J/cm³ for PAA [46]) Therefore, as the PVP binder dries, it is unable to resist the capillary pressures that pull the binder to the necking regions whereas the PVA binder can resist the capillary forces because it forms a crosslinked hydrogel [41]. Therefore, because of the attraction

of the polymer chains in solution, which can be characterized with the CED values, the binder might resist the capillary forces pushing it to the necking regions while drying.

Interestingly, there is only a 4.6 % difference between the CED of PVA and PAA (i.e. 519 J/cm^3 and 543 J/cm^3, respectively). Even if their CED values are similar, PVA forms a pendular interconnected network and PAA forms a coated network. Thus, the interactions of the polymer chains in solution can only partially explain the formation the different binder distributions. Therefore, whether the binder coats the particles or forms pendular bridges depends on the relation between polymer-solvent affinity (CED) and metal-polymer affinity (binding energy). In fact, PAA can form covalent bonds with the iron oxide present in the stainless steel surface [47] whereas PVA and PVP form hydrogen bonds with the hydroxilated oxide surface of the metal [48, 49]. Contrary to PVA and PVP, PAA samples could resist being immersed in water, which confirms that the interactions of PAA with the metal are much stronger. In the case of PVA and PVP, at low polymer concentrations, the -OH groups on the metal surface adsorb the solvent molecules (water, in this case) which form hydrogen bonds with the polymers [50]. As the water dries these bonds break and the polymers return to the solution. This is not the case with PAA, as the covalent bonds cannot be easily broken.

Evidently, if the binder is too viscous and has a low surface tension, capillary forces cannot transport the binder to the necking regions as it dries, which causes the binder to deposit over all the metallic surface (coated regime, Figure 8 c) [12]. However, this is not the case in our study, as can be seen in

Table 2, where the physicochemical properties of the binders used to prepare the top samples on Figure 10 are presented. In fact, the PVP forms pendular bridges even though it has similar properties to PAA. Also, PVA has the higher capillary number, which indicates that it is the worse binder to form pendular bridges. This clearly indicates that a binder can be in the coating regime even if it has a low surface tension and a high viscosity. These results also suggest that the coating behavior of PAA is not related to its physicochemical properties.

Table 2. Physicochemical properties of the 3 binders used to prepare 0.69 wt. % (C_g) samples.

Sample	Surface tension (mN/m)	Viscosity[*] (cP)	Ca[**] (eq. (1))
PVP	67.7 ± 0.1	8.3 ± 0.1	0.12
PVA	43.0 ± 0.1	16.1 ± 0.1	0.37
PAA	65.0 ± 0.1	10.7 ± 0.1	0.16

[*] Ambient temperature.
[**] Assuming a velocity of 1 m/s to simplify the units.

The SEM images of Figure 10 also show that the three binders fail by polymer decohesion. Particularly in the bottom images, one can see signs of ductile-brittle failure in the polymer phase for every binder (red arrows). This means that the strength of the PVP and PAA samples is also dictated by the binder phase strength, as was shown for PVA previously. In the case of

PAA, the samples do not reach their maximum possible strength (i.e. pure polymer strength) because of poor binder distribution (coated regime).

It has been shown that as C_b rises, the adsorption of the polymer onto the metallic oxide surface increases [21, 51]. At low C_b values, the adsorption is negligible. As C_b increases, the adsorption increases too up to a plateau value. Further increasing C_b does not change the amount of molecules adsorbed onto the metallic surface. This behavior impacts the formation of the first monolayer of polymer from which the bridges will initiate. It explains why PAA does not form a homogeneous coating at low C_b values (Figure 10). Initially, the concentration of PAA is too low to form this first monolayer, but as binder dries, the concentration increases, and a more significant adsorption takes place. Therefore, when the PAA concentration is sufficiently high to adsorb significantly into the surface, the liquid is no longer coating the entire particle. As a result, the polymer is not deposited evenly over all the metallic surface. It only forms homogenous coatings when the initial binder concentration is sufficiently high to start adsorbing onto the metal surface while the liquid is still coating the particles. The formation of that first polymer monolayer is another factor explaining why the exponential-like increase in the strength vs C_g curve is steeper for some binders. They reach adsorption saturation at different C_b values, as has been seen in other binder - powder systems [51].

Comparing the model curve of Figure 5 to the experimental values in Figure 9, one can observe that PAA presents the longest induction regime, followed by PVP and then, by PVA. This is expected, as PAA tends to deposit over the entire particle surface. Therefore, it takes higher PAA concentrations to form the first interparticle bridges. In the case of PVP, it readily

forms pendular bridges, which means that it has a short induction regime. However, PVP is significantly weaker than the other polymers. Thus, the exponential-like increase as a function of fill factor of this binder takes place at a lower rate, as weaker polymers form weaker interparticle bridges. In other words, PVP needs the accumulation of higher binder quantities than the other polymers to attain the same strength.

These results give us new insights into the characteristics of a good binder. First, it should have a narrow induction regime (i.e. a short Region A from Figure 3.2). The binder should form the first interparticle bridges and transit to Region B at the lowest possible fill factor, as Region B is the region of interest for BJP. Additionally, in Region B, a good binder would show a steep rise in properties as a function of the fill factor. In other words, it would have high pure polymer properties and would readily form a network of pendular bridges. Among the studied polymers, PVA is the one that best meets these performance criteria. Under these considerations, it is the best binder over PAA and PVP.

It is to be noticed however that depending on the application, PAA and PVP might be better suited. For instance, PVP is preferred for pharmaceutical applications because it is thermally, chemically and pH stable [19]. On its side, PAA is often used since it becomes water resistant after reacting with a ceramic or metallic surface [21]. Therefore, PAA printed green bodies become water resistant as well. Additionally, PAA displays a sudden change of properties in solution between pH = 4 − 6. In C_b= 5 % binder, we observed an increase of strength from 0.23 ± 0.08 to 6 ± 1 MPa in that pH range. In fact, due to its polyelectrolyte properties, PAA's carboxylic groups become predominantly negatively charged at pH = 5 or higher [52]. Since the metallic

surface is principally covered by OH_2^+ groups at high pHs [47, 53], the interactions between the polymer and the metal become stronger as pH increases.

That said, the addition of additives might also be detrimental to the green body's properties. For example, it is common use in BJP to add a proprietary ink to facilitate the observation of the binder with the naked eye [16, 29, 54]. However, we noticed that the strengths of PVA samples made with binders containing ink was drastically lower. In fact, pure polymer samples' strength decreased from 60 ± 10 MPa to 38 ± 6 when ink was added to the polymer. These results highlight the importance of assessing the impact of every new binder ingredient on the properties of the green bodies separately.

Proposed binder selection algorithm

The general goal is to obtain the highest green strength while using a minimum amount of binder, maintaining a high printing resolution and protecting the printhead. Considering this and the findings discussed before, the following selection algorithm is proposed (Figure 11).
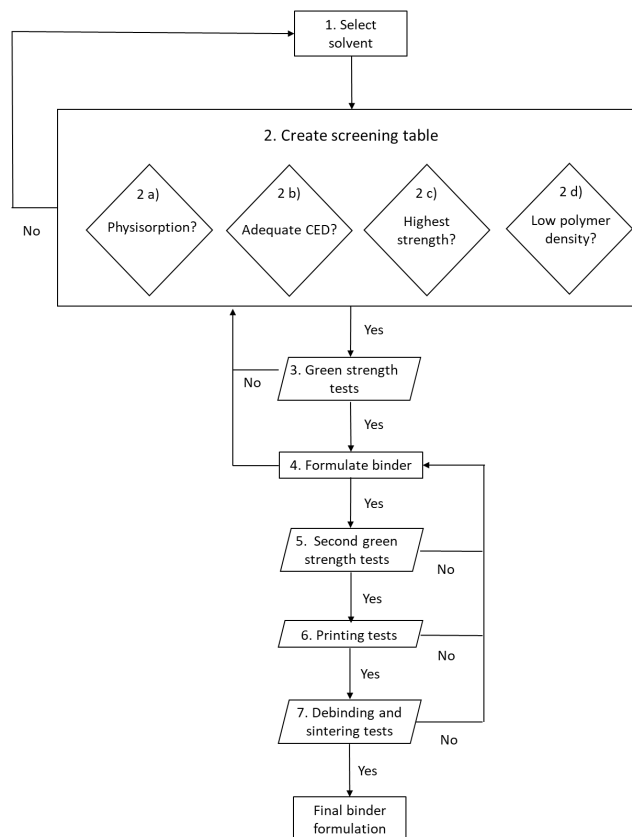
Figure 11. Binder selection algorithm based on model conditions. Squares represent process steps, diamonds, conditions, and parallelograms, testing operations. Diamonds inside one box need to be all respected.

For Step 1, the solvent selection, we suggest to use the approach of Tam et al. It consists in selecting the solvent considering the wettability of the powder bed by the solvent thanks to contact angles reported in the literature [20].

Step 2 consists in finding the adhesive agent of the binder by making a list of polymers that can be dissolved in the selected dispersing medium. The polymers are then screened using information found in the literature: interactions of the polymer with the metal (physisorption vs chemisorption), interactions of the polymer in solution (CED), polymer strength and

polymer density. Screening is done with a traffic light system: red = discarded, yellow = possible and green = good to move to next stage. Other parameters such as cost, degradation products, etc. can be considered at this stage.

Strong polymer-metal interactions lead to a coating binder distribution regime, as observed with the PAA binder. Therefore, physisorption is preferred over chemisorption (condition 2 a). Additionally, the affinity of the polymer chains with themselves in solution must not be too high, else the binder might not migrate to the necking regions properly, as was the case of PVA. With information of the CED one can keep track of the polymer-polymer affinity in solution. According to the results on PVP and PVA's binder distribution, a CED between 305 J/cm³ and 519 J/cm³ is acceptable, with values closer to the lower bound preferred (condition 2 b). Therefore, with the help of conditions 2 a and b, one can select the polymer candidates that promote the formation of a pendular network.

For polymer strength, tensile test data for pure polymer films (or other mechanical tests) are available in the literature. However, only data obtained with similar methods are comparable. One must choose the polymers with the highest strength, as shown with the cylindrical beam model, to obtain a steeper increase of green strength with respect to ϕ (condition 2 c). Additionally, candidates with the lowest densities are preferred, as a low density promotes the increase of the fill factor (condition 2 d). Thus, conditions 2 c and d allow the user to select the binding agents that form strong green bodies with small amounts of polymer. In other terms, a binder prepared with such polymers would show a narrow induction regime and a steep increase of strength in the exponential-like regime.

Step 3 consists in comparing the strengths of green bodies obtained with the polymers selected in Step 2. For this, binders prepared only with the solvent and the polymers are used to elaborate green bodies with different C_g values. For this, the out-of-printer approach and 0.2 % yield strength analysis are used. This stage allows the user to determine which polymer results in higher green strengths. Additionally, this process is important to explore the interval of ϕ values in the exponential-like regime. Knowing this interval of ϕ values, one can select C_b and C_g for the next steps.

Step 4 concerns the binder formulation. In order to elaborate a binder that respects the printer specifications, the use of the algorithms of Utela et al. [16] and Tam et al. [20] is recommended. These algorithms can be used namely for the selection of additives and co-solvents.

Step 5 is a series of experiments to screen the additives added to the formulation in Step 4 based on the mechanical properties of the green bodies (made with the out-of-printer method). One must prepare binders with one additive at the time. The resulting green strengths are compared to the values obtained without any additive in Step 3. Any ingredient that decreases the strength of the samples with respect to that obtained in Step 3, should be replaced, if possible.

Steps 6 and 7 were not the focus of this work and need to be further explored. That said, Step 6 is a printing test and formulation modification stage. It is to be noted that the printing parameters should be optimized for every binder with the help of existing methods [7, 16], else a comparison between the binders reaching this stage is not possible. Finally, for Step 7,

debinding and sintering tests must be accomplished to verify the quality of the final piece [8, 39, 55].

It is to be noted that this work is not intended to be a direct comparison to binder jetting. We developed an idealized case where the fundamental aspects of the formation of green bodies are accentuated. We propose an algorithm that extends beyond the scope of this research as a framework to be completed by future research. In fact, due to its complexity, the printing process must be studied in segments. This work is meant to be one of them.

Conclusion

This project aimed to develop binder selection guidelines through the investigation of the mechanical properties of SS 316L pieces prepared with PVP, PAA and PVA binders. A method to prepare model green bodies without using a binder jet printer was developed. The strength of the samples was carefully studied with compression tests and the 0.2 % yield strength was the principal property examined. The binder content in the green bodies was varied and studied with the help of the fill factor, ϕ, which is the percentage of empty volume in the piece occupied by dry binder.

The samples showed a quasi-sigmoidal trend of strength with respect to ϕ, which served to develop a model curve. The curve is divided in three regions: an induction regime, an exponential-like regime and a tail-off to a plateau value. In the induction regime, the binder starts depositing on the metallic surface without forming any interparticle bridge. The

exponential-like increase takes place due to an increase in the number of interparticle bridges formed and due to the coarsening of the bridges. Finally, the tail-off takes place because the remaining empty spaces between particles start getting filled by the binder.

PVP and PAA followed a similar trend to PVA. However, the rise of strength of the PVA green bodies was steeper, as it has higher pure polymer properties. On the other hand, PAA samples showed the lowest performance. SEM images showed in fact that PAA tended to coat the metallic particles. Therefore, not all the binder was used to give strength to the samples as opposed to PVP and PVA that formed pendular interparticle bridges. In the case of PVA, the binder tended to link the binder bridges with thin binder lines. These lines are probably formed because PVA has a higher cohesive energy density than the other polymers. On its side, PAA coating behavior might be explained by the higher affinity of this polymer with the metal surface. PAA forms covalent bonds with the metallic surface while PVP and PVA form hydrogen bonds.

A selection algorithm integrating all these findings is presented. The algorithm could facilitate the selection of binders for all kinds of applications in binder jetting as well as in other manufacturing fields such as metal injection moulding and direct ink writing. Additionally, the conceptual and fundamental understanding gained from this study will serve as guideline for printing parameter selection.

ASSOCIATED CONTENT

Supplementary Information

Additional details of the powder material; additional details on the distribution of the binder in the green body; Details for determining the interparticle bridge length.

AUTHOR INFORMATION

Corresponding Author

Sergio I. Yanez Sanchez - CREPEC, Department of Chemical Engineering, Polytechnique Montreal, Montréal, QC, H4T 1J4, Canada; Email: sergio-ivan.yanez-sanchez@polymtl.ca

Jason R. Tavares - CREPEC, Department of Chemical Engineering, Polytechnique Montreal, Montréal, QC, H4T 1J4, Canada; Email: jason.tavares@polymtl.ca

Author Contributions

The manuscript was written through contributions of all authors. All authors have given approval to the final version of the manuscript.

Notes

The authors declare no competing financial interest.

Acknowledgement

REFERENCES

(1) Gokuldoss, P. K.; Kolla, S.; Eckert, J., Additive manufacturing processes: Selective laser melting, electron beam melting and binder jetting—Selection guidelines. *Materials* **2017,** *10* (6), 672.

(2) Tofail, S. A.; Koumoulos, E. P.; Bandyopadhyay, A.; Bose, S.; O'Donoghue, L.; Charitidis, C., Additive manufacturing: Scientific and technological challenges, market uptake and opportunities. *Mater. today* **2018,** *21* (1), 22-37.

(3) Lee, J.-Y.; An, J.; Chua, C. K., Fundamentals and applications of 3D printing for novel materials. *Appl. Mater. Today* **2017,** *7*, 120-133.

(4) Mostafaei, A.; Elliott, A. M.; Barnes, J. E.; Li, F.; Tan, W.; Cramer, C. L.; Nandwana, P.; Chmielus, M., Binder jet 3D printing–process parameters, materials, properties, and challenges. *Prog. in Mater. Sci.* **2020**, 100707.

(5) Berger, R., Additive manufacturing: a game changer for the manufacturing industry. *Roland Berger Strategy Consultants GmbH, Munich* **2013,** *1* (5.1).

(6) Sachanandani, R. M.; Lombardo, S. J., Effect of green body size and heating rate on failure during thermal debinding and on the debinding cycle time. *J. Ceram. Process. Res.* **2011,** *12* (2), 115-121.

(7) Miyanaji, H.; Orth, M.; Akbar, J. M.; Yang, L., Process development for green part printing using binder jetting additive manufacturing. *Front. Mech. Eng.* **2018,** *13* (4), 504-512.

(8) Goffin, A. Caractérisation thermomécanique du frittage de poudre d'acier 316L mise en forme par jet de liant. Polytechnique Montréal, 2020.

(9) Salehi, M.; Maleksaeedi, S.; Nai, S. M. L.; Meenashisundaram, G. K.; Goh, M. H.; Gupta, M., A paradigm shift towards compositionally zero-sum binderless 3D printing of magnesium alloys via capillary-mediated bridging. *Acta Materialia* **2019,** *165*, 294-306.

(10) Utela, B.; Storti, D.; Anderson, R.; Ganter, M., A review of process development steps for new material systems in three dimensional printing (3DP). *J. Manuf. Process.* **2008,** *10* (2), 96-104.

(11) Sachs, E. M.; Hadjiloucas, C.; Allen, S.; Yoo, H. J., Metal and ceramic containing parts produced from powder using binders derived from salt. Google Patents: 2003.

(12) ONODA JR, G. Y., Theoretical strength of dried green bodies with organic binders. *J. Am. Ceram. Soc.* **1976,** *59* (5-6), 236-239.

(13) Miyanaji, H.; Zhang, S.; Yang, L., A new physics-based model for equilibrium saturation determination in binder jetting additive manufacturing process. *Int. J. Mach. Tools Manuf.* **2018,** *124*, 1-11.

(14) Salman, A. D.; Reynolds, G. K.; Tan, H. S.; Gabbott, I.; Hounslow, M. J., Breakage in granulation. In *Handb Powder Technol.*, Elsevier: 2007; Vol. 11, pp 979-1040.

(15) Gupta, S., A Perspective on Green Body Fabrication and Design for Sustainable Manufacturing. In *Green Sust. Manuf. Adv. Mater.*, Elsevier: 2016; pp 549-580.

(16) Utela, B. R.; Storti, D.; Anderson, R. L.; Ganter, M., Development Process for Custom Three-Dimensional Printing (3DP) Material Systems. *J. Manuf. Sci. Eng.* **2010,** *132* (1).

(17) Mao, Y.; Li, J.; Li, W.; Cai, D.; Wei, Q., Binder jetting additive manufacturing of 316 L stainless-steel green parts with high strength and low binder content: binder preparation and process optimization. *J. Mater. Process. Technol.* **2020**, 117020.

(18) Wilts, E. M.; Ma, D.; Bai, Y.; Williams, C. B.; Long, T. E., Comparison of Linear and 4-Arm Star Poly (vinyl pyrrolidone) for Aqueous Binder Jetting Additive Manufacturing of Personalized Dosage Tablets. *ACS Appl. Mater. Interfaces* **2019,** *11* (27), 23938-23947.

(19) Wilts, E. M.; Long, T. E., Thiol–ene addition enables tailored synthesis of poly (2-oxazoline)-graft-poly (vinyl pyrrolidone) copolymers for binder jetting 3D printing. *Polym. Int.* **2020,** *69* (10), 902-911.

(20) Tam, S. K.; Fung, K. Y.; Poon, G. S. H.; Ng, K. M., Product design: Metal nanoparticle-based conductive inkjet inks. *AIChE J.* **2016,** *62* (8), 2740-2753.

(21) Uhland, S. A.; Holman, R. K.; Morissette, S.; Cima, M. J.; Sachs, E. M., Strength of green ceramics with low binder content. *J. Am. Ceram. Soc.* **2001,** *84* (12), 2809-2818.

(22) Moon, J.; Grau, J. E.; Knezevic, V.; Cima, M. J.; Sachs, E. M., Ink-jet printing of binders for ceramic components. *J. Am. Ceram. Soc.* **2002,** *85* (4), 755-762.

(23) Williams, C. B.; Cochran, J. K.; Rosen, D. W., Additive manufacturing of metallic cellular materials via three-dimensional printing. *Int. J. Adv. Manuf. Technol.* **2011,** *53* (1), 231-239.

(24) Wei, Q.; Wang, Y.; Chai, W.; Zhang, Y.; Chen, X., Molecular dynamics simulation and experimental study of the bonding properties of polymer binders in 3D powder printed hydroxyapatite bioceramic bone scaffolds. *Ceram. Int.* **2017,** *43* (16), 13702-13709.

(25) Lores, A.; Azurmendi, N.; Agote, I.; Zuza, E., A review on recent developments in binder jetting metal additive manufacturing: materials and process characteristics. *Powder Metall.* **2019,** *62* (5), 267-296.

(26) Zhao, H.; Ye, C.; Xiong, S.; Fan, Z.; Zhao, L., Fabricating an effective calcium zirconate layer over the calcia grains via binder-jet 3D-printing for improving the properties of calcia ceramic cores. *Addit. Manuf.* **2020,** *32*, 101025.

(27) Zajic, L.; Buckton, G., The use of surface energy values to predict optimum binder selection for granulations. *Int. J. Pharm.* **1990,** *59* (2), 155-164.

(28) Trenfield, S. J.; Madla, C. M.; Basit, A. W.; Gaisford, S., Binder jet printing in pharmaceutical manufacturing. In *3D Printing of Pharmaceuticals*, Springer: 2018; pp 41-54.

(29) LEWIS, R. M., Powder binder interactions in 3D inkjet printing. **2014**.

(30) Huang, S.; Ye, C.; Zhao, H.; Fan, Z.; Wei, Q., Binder jetting yttria stabilised zirconia ceramic with inorganic colloid as a binder. *Adv. Appl. Ceram.* **2019,** *118* (8), 458-465.

(31) de Castro Costa, R. P.; de Oliveira, D. A. L.; Marciano, F. R.; Trava-Airoldi, V. J., Tribological Behavior of DLC Films in Space and Automotive Oil under Boundary Lubrication. *J. Aerosp. Eng.* **2012,** *4* (1), 104.

(32) Patirupanusara, P.; Suwanpreuk, W.; Rubkumintara, T.; Suwanprateeb, J., Effect of binder content on the material properties of polymethyl methacrylate fabricated by three dimensional printing technique. *J. Mater. Process. Technol.* **2008,** *207* (1-3), 40-45.

(33) Ohring, M., *Eng. Mater. Sci*. Elsevier: 1995.

(34) Mitchell, B. S., *An introduction to materials engineering and science for chemical and materials engineers*. John Wiley & Sons: 2004.

(35) van Liempt, P.; Sietsma, J., A physically based yield criterion I. Determination of the yield stress based on analysis of pre-yield dislocation behaviour. *Mater. Sci. Eng. A* **2016,** *662*, 80-87.

(36) Gilmer, D.; Han, L.; Hong, E.; Siddel, D.; Kisliuk, A.; Cheng, S.; Brunermer, D.; Elliott, A.; Saito, T., An in-situ crosslinking binder for binder jet additive manufacturing. *Addit. Manuf.* **2020**, 101341.

(37) Willett, C. D.; Johnson, S. A.; Adams, M. J.; Seville, J. P., Pendular capillary bridges. In *Handb. Powder Technol.*, Elsevier: 2007; Vol. 11, pp 1317-1351.

(38) Melcher, R.; Travitzky, N.; Zollfrank, C.; Greil, P., 3D printing of Al_2O_3/Cu–O interpenetrating phase composite. *J. Mater. Sci.* **2011,** *46* (5), 1203-1210.

(39) Do, T.; Kwon, P.; Shin, C. S., Process development toward full-density stainless steel parts with binder jetting printing. *Int. J. Mach. Tools Manuf.* **2017,** *121*, 50-60.

(40) Kobayashi, M.; Hyu, H. S., Development and evaluation of polyvinyl alcohol-hydrogels as an artificial atrticular cartilage for orthopedic implants. *Materials* **2010,** *3* (4), 2753-2771.

(41) Liu, T.; Peng, X.; Chen, Y. N.; Bai, Q. W.; Shang, C.; Zhang, L.; Wang, H., Hydrogen-bonded polymer–small molecule complexes with tunable mechanical properties. *Macromol. Rapid Commun.* **2018,** *39* (9), 1800050.

(42) Gaaz, T. S.; Sulong, A. B.; Akhtar, M. N.; Kadhum, A. A. H.; Mohamad, A. B.; Al-Amiery, A. A., Properties and applications of polyvinyl alcohol, halloysite nanotubes and their nanocomposites. *Molecules* **2015,** *20* (12), 22833-22847.

(43) Peng, C.; Chen, G., Preparation and assessment of heat-treated α-chitin nanowhiskers reinforced poly (viny alcohol) film for packaging application. *Materials* **2018,** *11* (10), 1883.

(44) Liu, R.; Du, J.; Zhang, Z.; Li, H.; Lu, J.; Cheng, Y.; Lv, Y.; Wang, H., Preparation of polyacrylic acid-grafted-acryloyl/hemicellulose (PAA-g-AH) hybrid films with high oxygen barrier performance. *Carbohydr. polym.* **2019,** *205*, 83-88.

(45) Liu, C.; Xiao, C.; Liang, H., Properties and structure of PVP–lignin "blend films". *J. Appl. Polym. Sci.* **2005,** *95* (6), 1405-1411.

(46) He, Q.; Liu, J.; Liang, J.; Liu, X.; Tuo, D.; Li, W., Chemically surface tunable solubility parameter for controllable drug delivery—an example and perspective from hollow PAA-coated magnetite nanoparticles with R6G model drug. *Materials* **2018,** *11* (2), 247.

(47) Raman, A.; Quiñones, R.; Barriger, L.; Eastman, R.; Parsi, A.; Gawalt, E. S., Understanding organic film behavior on alloy and metal oxides. *Langmuir* **2010,** *26* (3), 1747-1754.

(48) Kayal, S.; Ramanujan, R., Doxorubicin loaded PVA coated iron oxide nanoparticles for targeted drug delivery. *Mater. Sci. Eng.: C* **2010,** *30* (3), 484-490.

(49) Koczkur, K. M.; Mourdikoudis, S.; Polavarapu, L.; Skrabalak, S. E., Polyvinylpyrrolidone (PVP) in nanoparticle synthesis. *Dalton Trans.* **2015,** *44* (41), 17883-17905.

(50) Merişanu, C.; Samide, A.; Iacobescu, G. E.; Tutunaru, B.; Tigae, C.; Popescu, A., Anticorrosive Performance of Vinyl Butyral-co-vinyl alcohol-co-vinyl Acetate Based Copolymer Adsorbed on Steel Surfaces. Electrochemical and AFM Studies. *Int. J. Electrochem. Sci* **2020,** *15*, 10197-10211.
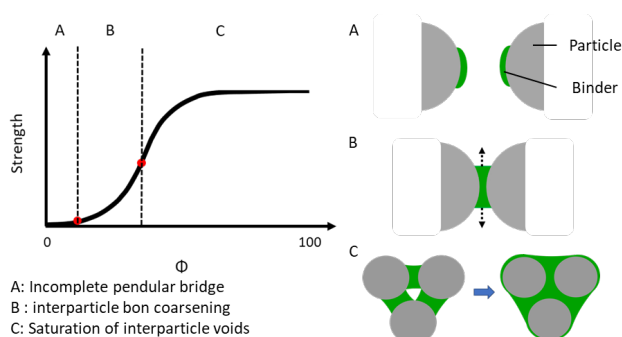
(51) Romdhane, M. R. B.; Chartier, T.; Baklouti, S.; Bouaziz, J.; Pagnoux, C.; Baumard, J.-F., A new processing aid for dry-pressing: a copolymer acting as dispersant and binder. *J. Eur. Ceram. Soc.* **2007,** *27* (7), 2687-2695.

(52) Swift, T.; Swanson, L.; Geoghegan, M.; Rimmer, S., The pH-responsive behaviour of poly (acrylic acid) in aqueous solution is dependent on molar mass. *Soft Matter* **2016,** *12* (9), 2542-2549.

(53) McCafferty, E., Acid-Base Properties of Surface Oxide Films. In *Surface Chemistry of Aqueous Corrosion Processes*, Springer: 2015; pp 1-54.

(54) Lam, C. X. F.; Mo, X.; Teoh, S.-H.; Hutmacher, D., Scaffold development using 3D printing with a starch-based polymer. *Mater. Sci. Eng.: C* **2002,** *20* (1-2), 49-56.

(55) Wang, Y.; Zhao, Y. F., Investigation of Sintering Shrinkage in Binder Jetting Additive Manufacturing Process. *Procedia Manuf.* **2017,** *10*, 779-790.

For table of contents only